Journal of Thermal Analysis and Calorimetry (2022) 147:6403–6414
https://doi.org/10.1007/s10973-021-10975-0

Experimental study of the phase relations and thermodynamic properties of Bi-Se system

Gunel S. Hasanova[1] · Aytan I. Aghazade[2] · Dunya M. Babanly[3,4] · Samira Z. Imamaliyeva[2] · Yusif A. Yusibov[1] · Mahammad B. Babanly[2]

Received: 28 January 2021 / Accepted: 29 June 2021 / Published online: 10 July 2021

Abstract
The Bi-Se system was studied by differential thermal analysis, powder X-ray diffraction, scanning electron microscopy, as well as by electromotive forces (EMF) measurements of electrochemical cells (−) Bi (solid) | ionic liquid + Bi^{3+} | Bi-Se (solid) (+). A new refined version of the phase diagram reflecting the compounds Bi_2Se_3, Bi_3Se_4, Bi_8Se_9, BiSe, Bi_8Se_7, Bi_4Se_3, and Bi_3Se_2 with almost constant composition was constructed. It was established that the first compound melts congruently, and all the rest melt with peritectic reaction. The types and parameters of the crystal lattices of the above-mentioned compounds were determined based on the powder diffraction patterns. From the EMF measurements, the partial molar functions of bismuth in alloys and the standard integral thermodynamic functions of bismuth selenides were calculated. Comparative analysis of the obtained results with the literature data is carried out.

Keywords Bismuth selenides · Phase diagram · Incongruent melting · Tetradymite-like structure · Electromotive force method · Thermodynamic properties

Introduction

Layered bismuth selenides, especially Bi_2Se_3, as well as doped phases and solid solutions based on it, are objects of numerous studies as valuable materials exhibiting unique optical, thermoelectric, and other functional properties. This makes them promising for use in various thermoelectric and photoelectrochemical devices, broadband and high-speed optoelectronics, etc. [1–8]. The discovery of a topological insulator (TI), a new quantum state of matter [9, 10], led to a sharp increase in attention to layered narrow-gap semiconductors, in particular, bismuth selenides and tellurides. The results of several studies have shown that these phases exhibit the properties of TI [11–16] and can be used in spintronics, quantum computers, medicine, security systems, etc. [17–20].

The valid data on phase equilibria and thermodynamic functions of the corresponding systems are required for the development of synthesis methods and optimization of the conditions for the preparation of novel materials [20–23].

The known versions of the phase diagrams of the Bi-Se system (see Fig. S1), constructed in different periods of the last century, differ significantly from each other. The first version of the T-x diagram of this system, given in the handbook [24], is constructed based on the data [25, 26] obtained at the beginning of the last century. According to this diagram (Fig.S1a), the system was characterized by the formation of two compounds—Bi_2Se_3 and BiSe, melting congruently (979 K) and incongruently (878 K), respectively. The second version (Fig. S1b) was built by Abrikosov et al. [27] based on DTA and microstructure analysis results of samples subjected to long-time (3000–3600 h) thermal annealing at 520 K. This diagram reflects three compounds Bi_2Se_3, BiSe, and Bi_2Se. The former melts congruently at 979 K, the latter two decompose by peritectic reactions at 880 and 741 K, respectively. In addition, it was defined that BiSe is a compound with variable composition and has a wide

✉ Mahammad B. Babanly
babanlymb@gmail.com

1 Ganja State University, AZ-2000 Ganja, Azerbaijan

2 Institute of Catalysis and Inorganic Chemistry, ANAS, AZ-1143 Baku, Azerbaijan

3 Azerbaijan State Oil and Industry University, AZ-1010 Baku, Azerbaijan

4 French-Azerbaijani University (UFAZ), AZ-1010 Baku, Azerbaijan

(41.3–55.5 at.% Se) homogeneity range [27]. In [28], the existence of Bi_2Se was disputed and it was shown that the compound richest in bismuth has the composition Bi_3Se_2, and the homogeneity region of BiSe is 46–56 at.% Se. The results of works [29, 30] do not agree with the data [24, 27]. Thus, in [29], based on the XRD data of selected alloys, the existence of three compounds Bi2Se, BiSe, and Bi_2Se_3 was shown, between which continuous solid solutions are formed. The same opinion is expressed in [30]. The authors of [31] presented another version of the phase diagram of the Bi-Se system based on DTA, XRD, microstructural analysis, and local X-ray spectral analysis of alloys annealed at 500 K for 1200 h (3000 h for a number of samples). This diagram practically coincides with the data of [27], the only difference that instead of the Bi_2Se compound, the formation of the Bi_3Se_2 compound with incongruent melting at 743 K is indicated, and the homogeneity region of BiSe covers the composition range 42.5–54.5 at.% Se.

With that, a number of works [32–37] devoted to the synthesis and study of the crystal structure of several bismuth selenides, including those not reflected in the phase diagram were published. Based on the summary of the available data, Okamoto presented [38] a compiled phase diagram (Fig. S1 c), reflecting the compositions of all known and supposed bismuth selenides. As can be seen from this diagram, the author attributed the peritectic reactions at 743 and 880 K to the Bi_3Se_2 and Bi_4Se_5, respectively, and the question regarding the temperature and melting character of other bismuth selenides remained open.

Analysis of the literature data also shows that thermodynamic functions were determined only for Bi_2Se_3 and BiSe [39–45]. Some works [46–48] present the results of modeling and thermodynamic analysis of the Bi-Se phase diagram, in particular, by the CALPHAD method in the approximation of the associated solution model. However, these studies do not consider the $nBi_2{\cdot}mBi_2Se_3$ homologous series as individual compounds.

Therefore, we undertook a repeated comprehensive study of the phase relations and thermodynamic functions of the Bi-Se system. The results of the solid-phase equilibria study in the 50–65 at.% Se composition range and the thermodynamic properties of Bi_2Se_3, Bi_3Se_4, Bi_8Se_9, and BiSe were presented in [49].

The present work aimed to refine the phase diagram of the Bi-Se system in the composition range of 0–60 at.% Se and to study the thermodynamic properties of lower bismuth selenides; Bi_8Se_7, Bi_4Se_3, and Bi_3Se_2.

Experimental

Synthesis

The alloys for the study were synthesized by fusion of high-purity elemental bismuth (99.999%) and selenium (99.999%) purchased from Alfa Aesar (Germany) in evacuated (~ 10^{-2} Pa) quartz ampoules.

When developing the synthesis methodology of samples, we proceeded from the results of numerous studies that the bulk samples of layered phases obtained by the widely used fusion method do not reach an equilibrium state even after a prolonged (2000–3000 h) thermal annealing [27, 28, 31, 50, 51]. This is apparently because, unlike conventional bulk samples, Van der Waals phases obtained in non-equilibrium crystallization conditions (i.e., ordinary cooling of the melt) practically do not undergo any changes during further heat treatment due to very low diffusion between layers.

Taking this into account, to ensure a high dispersion of samples, after alloying, some of them (series I) were quenched by dropping ampoules into ice water from a liquid state (1000 K), followed by annealing at 700 K (1000 h) and 400 K (20 h). For comparison, some alloys with selective compositions (series II) were synthesized by the traditional fusion method and annealed under similar conditions.

Methods

Studies were carried out by the differential thermal (DTA), powder X-ray phase diffraction (PXRD), scanning electron microscopy (SEM), and electromotive force (EMF) methods.

DTA was performed using a NETZSCH 404 F1 Pegasus differential scanning calorimeter. The crystal structure was analyzed by a powder X-ray diffraction (PXRD) technique at room temperature using a Bruker D8 diffractometer (CuK_α radiation) in the range of $2\theta = 10–70°$. High-resolution SEM images were recorded using a TESCAN VEGA3 SBH instrument.

For the thermodynamic studies, the EMF of the concentration cells of the type

$$(-)\mathrm{Bi(Solid)|ionicliquid} + \mathrm{Bi^{3+}|Bi\text{-}Se\ (Solid)}\ (+) \quad (1)$$

was measured in the 300–450 K temperature range.

Various modifications of the EMF method and different electrolytes (solid and liquid) are successfully used for the thermodynamic study of inorganic systems [52–68]. When

studying metal sulfides and selenides, EMF measurements should be carried out at temperatures below the solidus of the corresponding system. The results of a number of works [44, 55, 56, 63–66] have shown that for such measurements, the most suitable electrolytes were glycerol solutions of halides of alkali and alkaline earth metals. We have shown that in such low-temperature measurements, ionic liquids can also be used as electrolytes [67, 68].

Alloys with the composition of 42–48 at.% Se of series (I) were used as right (positive) electrodes, while the elementary bismuth was used as a negative electrode in the cells of the type (1). The prepared alloys consisted of the following two-phase mixtures: $Bi_8Se_7 + BiSe$, $Bi_4Se_3 + Bi_8Se_7$ or $Bi_3Se_2 + Bi_4Se_3$. Note that, despite the fact that we failed to obtain a homogeneous sample of the Bi_3Se_2 compound, the alloys with the compositions 42.0 and 42.7 at.% Se were two-phase ($Bi_3Se_2 + Bi_4Se_3$) and did not contain traces of elemental bismuth.

An ionic liquid (morpholine formate) with the addition of $BiCl_3$ was used as an electrolyte. In [69], the conductivities of the morpholinium cation-based protic ionic liquids were measured in the 0–100 °C temperature range and it was shown that morpholine formate has a fairly high (9.92 mS cm^{-1} at 60 °C and 29 mS cm^{-1} at 100 °C) pure ionic conductivity. To obtain the ionic liquid, we used morpholine (CAS No.110–91-8), formic acid (CAS No. 64–18-6), and anhydrous $BiCl_3$ (CAS No.7787–60-2) purchased from Alfa Aesar (Germany). A detailed description of the method for obtaining an ionic liquid is given in [68, 69]. We have assembled electrochemical cells, the designs of which are described in detail in the works [67, 68].

The first equilibrium EMF values were obtained after holding the concentration cell at ~ 350 K for ~ 40–60 h, and the subsequent ones every 3–4 h after a certain temperature were established. In the entire temperature range of measurements, reproducible EMF values were obtained. The EMF values that did not differ from each other during repeated measurements at a given temperature by more than 0.2 mV, regardless of the direction of temperature change, were recorded as equilibrium values. During the experiment, the EMF of each sample was measured three times at two constant temperatures. For example, for an alloy from the $Bi_8Se_7 + BiSe$ phase region at 350.6 K, EMF values were 90.95, 91.99, and 91.29 mV Table 1 presents the averaged value of 91.11 mV.

Table 1 Nonvariant equilibria in the Bi-$Bi_{0.4}Se_{0.6}$ system

Point in Fig. 4	Equilibria	T, K	Composition, at % Se
P_1	$L + Bi_2Se_3 \leftrightarrow Bi_3Se_4$	890	51
P_2	$L + Bi_3Se_4 \leftrightarrow Bi_8Se_9$	881	50
P_3	$L + Bi_8Se_9 \leftrightarrow BiSe$	866	48.5
P_4	$L + BiSe \leftrightarrow Bi_8Se_7$	853	43.5
P_5	$L + Bi_8Se_7 \leftrightarrow Bi_4Se_3$	829	40
P_6	$L + Bi_4Se_3 \leftrightarrow Bi_3Se_2$	742	20
E	$L \leftrightarrow Bi + Bi_3Se_2$	540	2

Results and discussion

Phase relations

The study of both series alloys has shown that samples of series (I) are closer to the equilibrium state than samples of series (II).

The results of XRD analysis of alloys of series (I) in the 50–60 at.% Se composition range including compounds Bi_2Se_3, Bi_3Se_4, Bi_8Se_9, BiSe are presented and discussed in [49]. The PXRD patterns of some alloys with high bismuth contents are shown in Figs. 1 and 2. As can be seen, alloys with the compositions Bi_8Se_7 and Bi_4Se_3 (Fig. 1) are single-phase, while the alloy with the Bi_3Se_2 composition (Fig. 2a) is three-phase and in addition to Bi_3Se_2 contains Bi_4Se_3 and elemental bismuth. We have also found that intermediate alloys between stoichiometric compounds are two-phase. As an example, Fig. 2b, c shows powder diffraction patterns of samples with the compositions 42 and 45 at.% Se. As can be seen, they consist of two-phase mixtures $Bi_3Se_2 + Bi_4Se_3$ and $Bi_8Se_7 + Bi_4Se_3$, respectively. Note that, the absence of other phases in these alloys is an additional feature of their equilibria.

The types and parameters of crystal lattices of bismuth selenides (Table S1) determined based on analysis of diffraction patterns using the TOPAS 4.2 software are in good agreement with the literature data [31–37].

The results of SEM analysis were in agreement with the XRD data. As an example, Fig. 3 shows the SEM patterns of alloys with 42.9 and 46.7 at.% Se contents, corresponding to

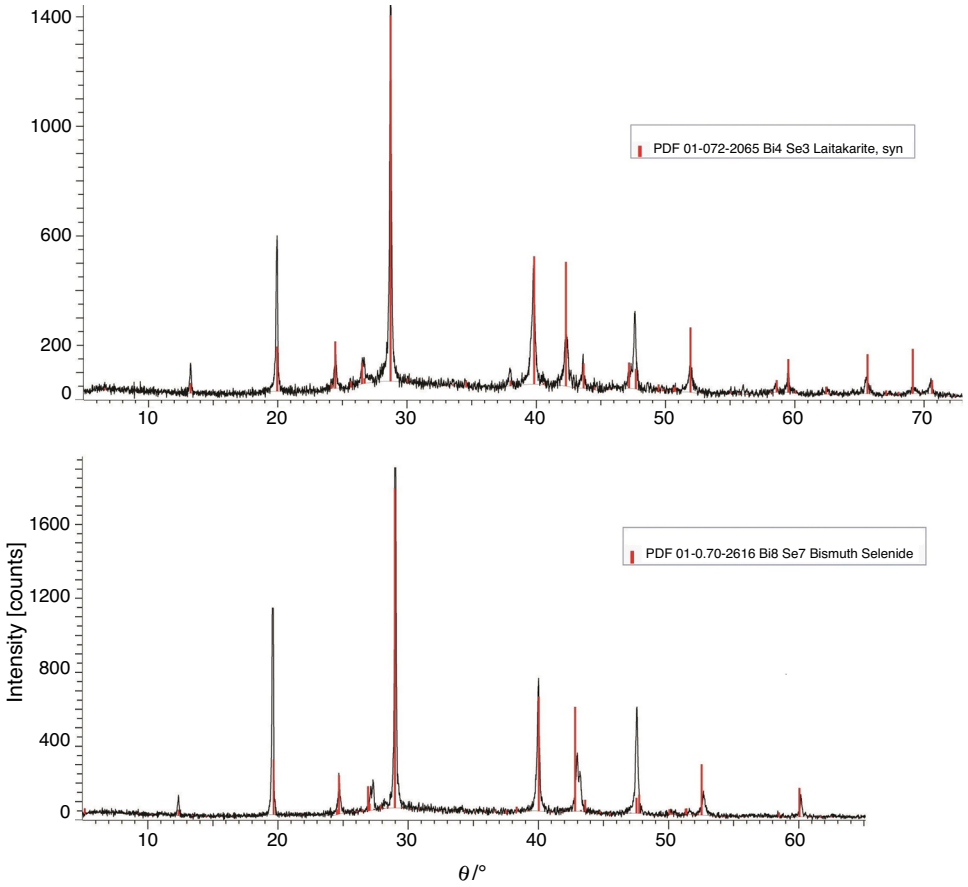

Fig. 1 The PXRD patterns of Bi_8Se_7 and Bi_4Se_3 compounds

the stoichiometry of Bi_4Se_3 and Bi_8Se_7. As can be seen, both samples are single-phase and have alike layered structures.

Based on the DTA and XRD data, we constructed a phase diagram of the Bi-Se system in the 0–60 at.% Se composition range (Fig. 4). This diagram reflects seven bismuth selenides: Bi_2Se_3 melts congruently at 978 K, the other six compounds melt with decomposition by peritectic reactions (Table 1).

Comparison of Fig. 4 with the previously constructed versions (Fig. S1) of the Bi-Se phase diagram shows that all three compounds (Bi_3Se_2, BiSe и Bi_2Se_3) indicated in [28, 31] (Fig. S1,b) were confirmed in this work. Moreover, the temperature of the peritectic decomposition of Bi_3Se_2 (742 K) practically coincides with the literature data. The peritectic temperature for BiSe (866 K) determined by us is somewhat lower than that given in [27, 28, 31] (873–879 K). A wide homogeneity region of BiSe has not been confirmed by us. Instead, in the "homogeneity" region (42–55.5 at.% Se) of this compound, four individual phases (Bi_4Se_3, Bi_8Se_7, BiSe, and Bi_8Se_9) were revealed (Fig. S1, Table 1).

The DTA heating curves of some samples of series I are presented in Fig. 5 and series II in Fig. 6, while the cooling curves are shown in Fig. 7. As can be seen in Fig. 5, the heating curves of this series of alloys are in full agreement with the T-x diagram (Fig. 4). Endothermic effects at 829, 866, and 881 K are related to the temperatures of peritectic decomposition of Bi_4Se_3, BiSe, and Bi_8Se_9, respectively. The intermediate effect at 890 K (Fig. 5,c) corresponds to the peritectic decomposition, while at 928 K to the liquidus.

DTA heating curves of alloys of series II with the same composition (Fig. 6) have a slightly different form. For example, in Fig. 6, thermal effects are corresponding to the eutectic melting (540 K) and the peritectic decomposition of Bi_3Se_2, which do not exist in Fig. 5a. In addition, the weakest endothermic effect in the 823–853 K range is in better agreement with the phase diagram given in Fig. S-1b. The heating curves (Fig. 6) also contain *several overlapping endothermic* effects, that are absent in the curves in Figs. 5 b,c which indicates that alloys of series II are in a non-equilibrium state.

DTA cooling curves provide very useful information (Fig. 7). Note that, as expected, they were the same for alloys of both series. On the other hand, there are several exothermic effects on the cooling curves (Fig. 7) after the onset of crystallization, which do not agree with the data (Fig. 1b) about the presence of a wide range of solid solutions based on BiSe. These curves are in better agreement with the heating curves for samples of series II (Fig. 6).

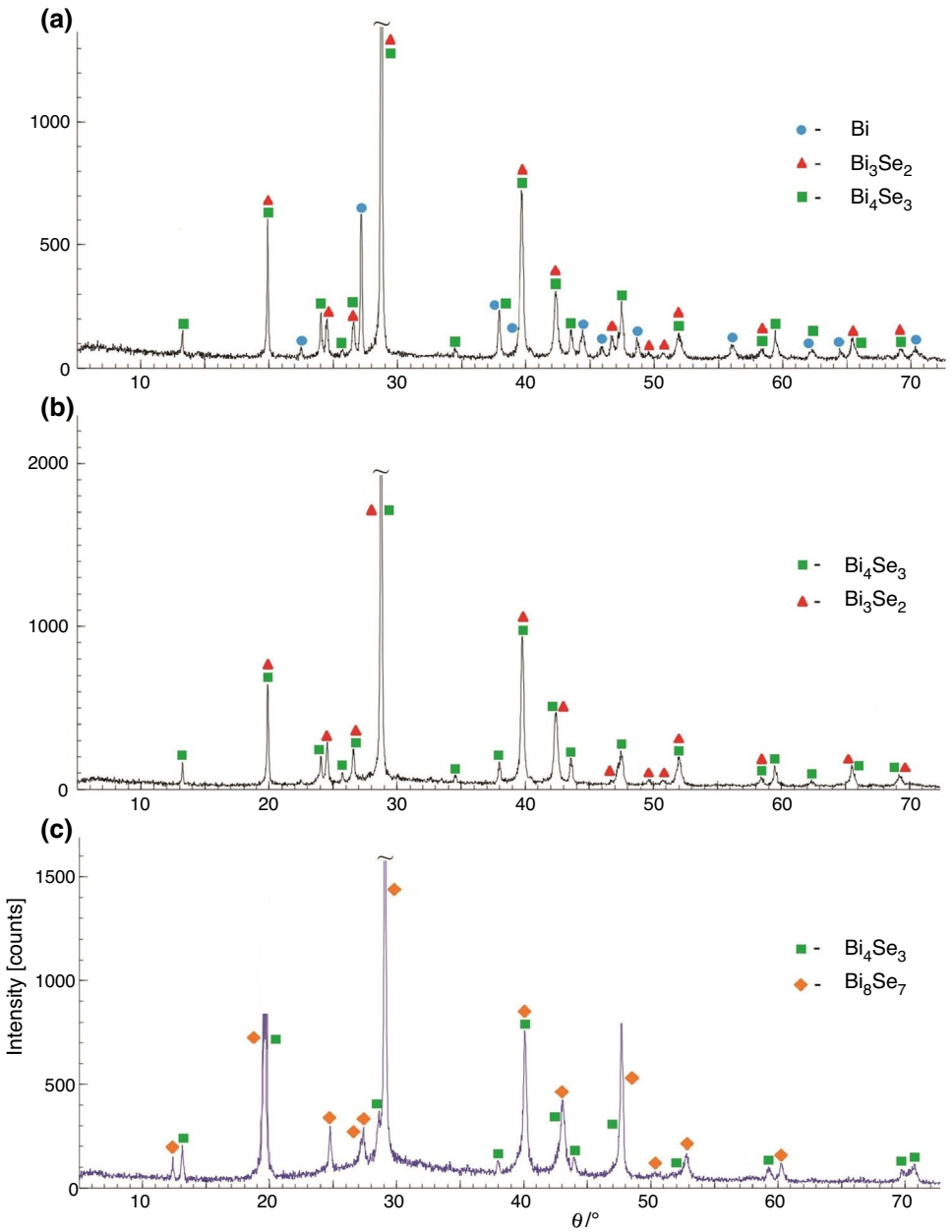

Fig. 2 The PXRD patterns of alloys of the Bi-Se system with the compositions 40 (**a**), 42 (**b**) and 45 at.% Se (**c**)

Thus, a comparison of Figs. 5–7 shows that the data presented in Fig. 5 are close to equilibrium, while Figs. 6 and 7 reflect non-equilibrium states and processes. Thermal effects on the cooling curves reflect the series of peritectic formation reactions of the compounds indicated in the phase diagram (Fig. 4). Since, when the samples are cooled, these reactions do not proceed completely and pass into other lower-temperature reactions, including absent in the equilibrium diagram. The closeness of the character of these curves to the heating curves of the series II samples shows that despite prolonged annealing, samples of this series are far from the equilibrium state. This confirms the data [50, 51] on the inefficiency of thermal annealing of coarse-crystalline mixtures of phases with a layered structure.

In conclusion, it should be noted that a comparison of the constructed phase diagram (Fig. 4) with the compiled phase diagram [38] shows that 8 out of 15 compounds indicated in this diagram were not confirmed by us. It should also be noted that according to [38], the Bi_3Se_2 and Bi_3Se_4 compounds melt incongruently at 743 and 880 K, as well as the character and melting point of other compounds were not indicated at all. In the T-x phase diagram constructed by us, the peritectic temperature of Bi_3Se_4 is slightly higher (890 K), and the horizontal at 881 K refers to Bi_8Se_9.

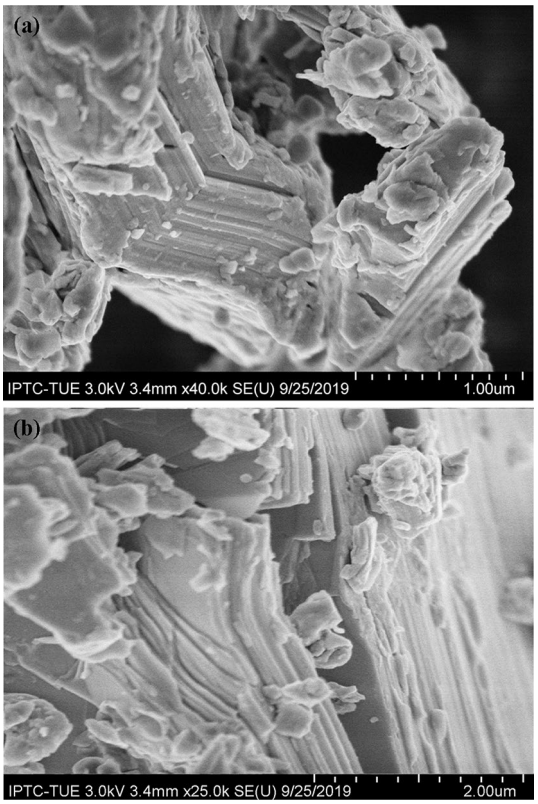

Fig. 3 SEM patterns of alloys with 42.9 and 46.7 at.% Te contents

Thermodynamic properties

EMF measurements data of cells of type (1) were in agreement with the constructed phase diagram (Fig. 4). This allows using them for thermodynamic calculations. The EMF measurements for alloys in the 50–65 at.% Se composition range are presented and processed in [49].

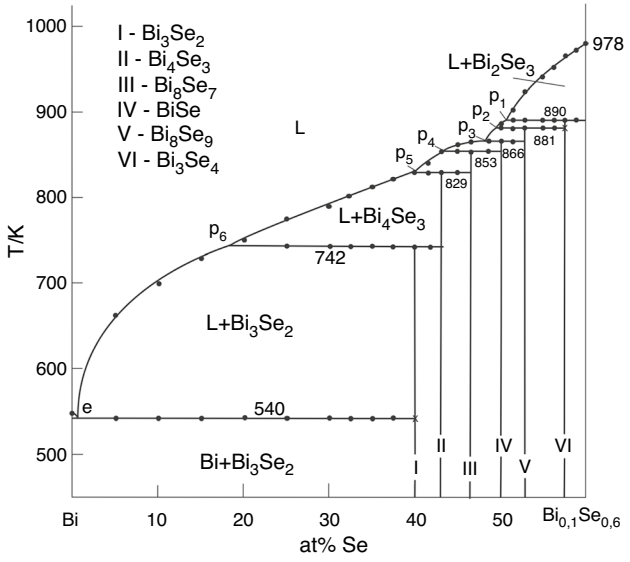

Fig. 4 Phase diagram of the Bi-Se system in the 0–60 at.% Se composition range

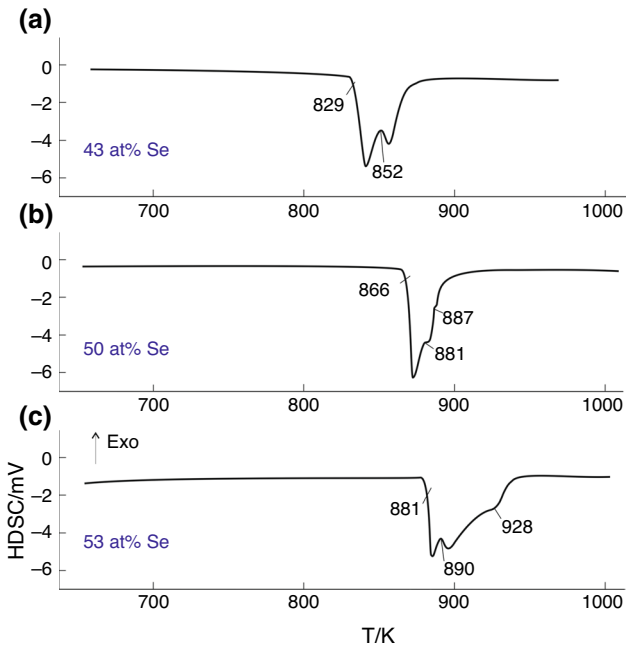

Fig. 5 DTA heating curves of some samples of series I

E and T pairs of values for the alloys from the 42–48 at.% Se composition range are shown in Table 2, and the corresponding graphs of temperature dependences of EMF are shown in Fig. 8. Taking into account the linearity of these dependencies, they were processed using the Microsoft Office Excel 2003 software by the least squares method. The linear equations obtained are given in Table 3 in the form recommended in [53, 54]

$$E = a + bT \pm t\left[\frac{\delta_E^2}{n} + \delta_b^2(T-\overline{T})^2\right]^{1/2} \quad (2)$$

In Eq. (2), a and b are coefficients, n is the number of pairs of E and T values; $\overline{T}$ is the average temperature, K; t Student's t test, and T is the temperature, K. δ_E^2 and δ_b^2 are dispersions of individual EMF values and the constant b. Considering the number of experimental points, $n = 30$, at a confidence level of 95%, the Student's test is $t \leq 2$.

From equations (Table 3) using thermodynamic relationships [52, 53]

$$\overline{\Delta G}_{Bi} = -zFE \quad (3)$$

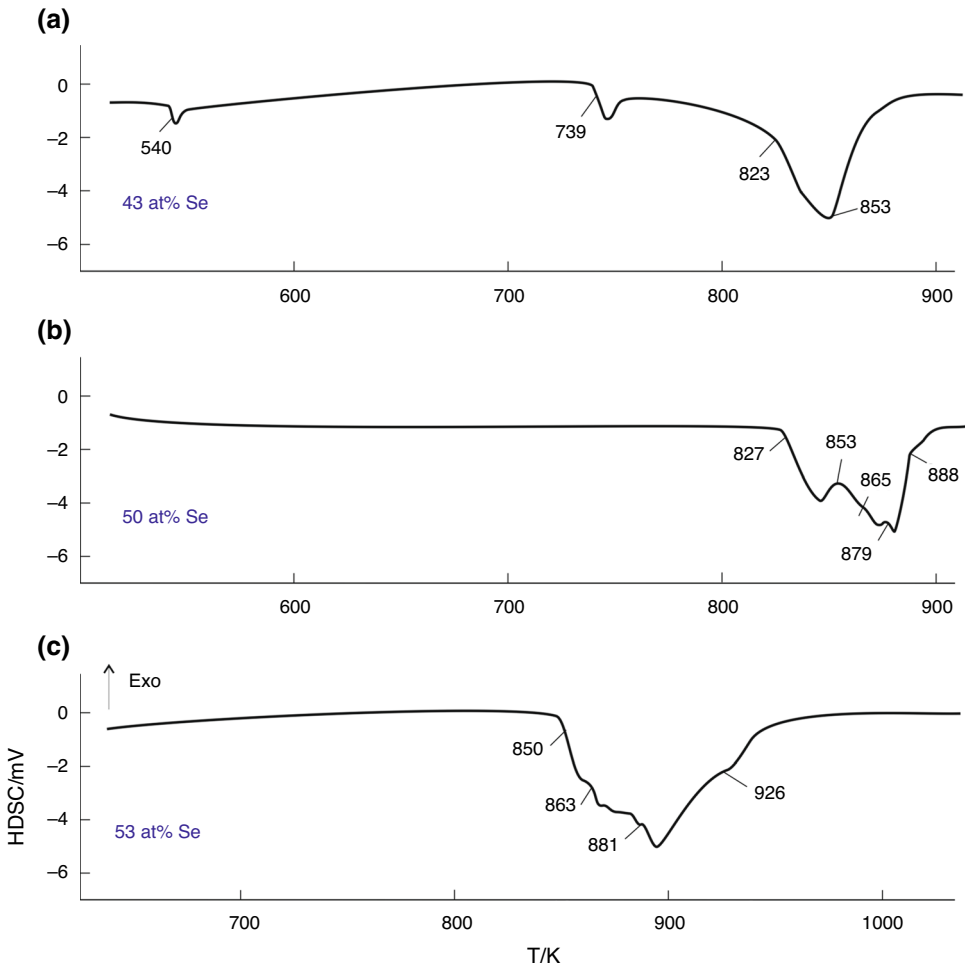

Fig. 6 DTA heating curves of some samples of series II

$$\overline{\Delta S}_{\mathrm{Bi}} = zF\left(\frac{\partial E}{\partial T}\right)_{\mathrm{P}} = zFb \tag{4}$$

$$\overline{\Delta H}_{\mathrm{Bi}} = -zF\left[E - T\left(\frac{\partial E}{\partial T}\right)_{\mathrm{P}}\right] = -zFa \tag{5}$$

the partial molar Gibbs free energy, enthalpy, and entropy of bismuth in alloys were calculated (Table 4). Because, Bi_8Se_7, Bi_4Se_3, and Bi_3Se_2 compounds have an almost constant composition, the above-mentioned partial molar values are thermodynamic functions of the following potentialforming reactions (the physical state of substances is crystalline) [53, 54]:

$$\mathrm{Bi} + 7\mathrm{BiSe} = \mathrm{Bi_8Se_7} \tag{6}$$

$$\mathrm{Bi} + 0.75\ \mathrm{Bi_8Se_7} = 1.75\mathrm{Bi_4Se_3} \tag{7}$$

$$\mathrm{Bi} + 2\mathrm{Bi_4Se_3} = 3\mathrm{Bi_3Se_2} \tag{8}$$

From relationships (6)–(8) according to the expressions

$$\Delta_{\mathrm{f}}Z^0(Bi_8Se_7) = \overline{\Delta Z_{\mathrm{Bi}}} + 7\Delta_{\mathrm{f}}Z^0(BiSe) \tag{9}$$

$$\Delta_{\mathrm{f}}Z^0(Bi_4Se_3) = \frac{4}{7}\overline{\Delta Z_{\mathrm{Bi}}} + \frac{3}{7}\Delta_{\mathrm{f}}Z^0(Bi_8Se_7) \tag{10}$$

$$\Delta_{\mathrm{f}}Z^0(Bi_3Se_2) = \frac{1}{3}\overline{\Delta Z_{\mathrm{Bi}}} + \frac{2}{3}\Delta_{\mathrm{f}}Z^0(Bi_4Se_3) \tag{11}$$

the standard Gibbs free energy and the enthalpy of formation and from

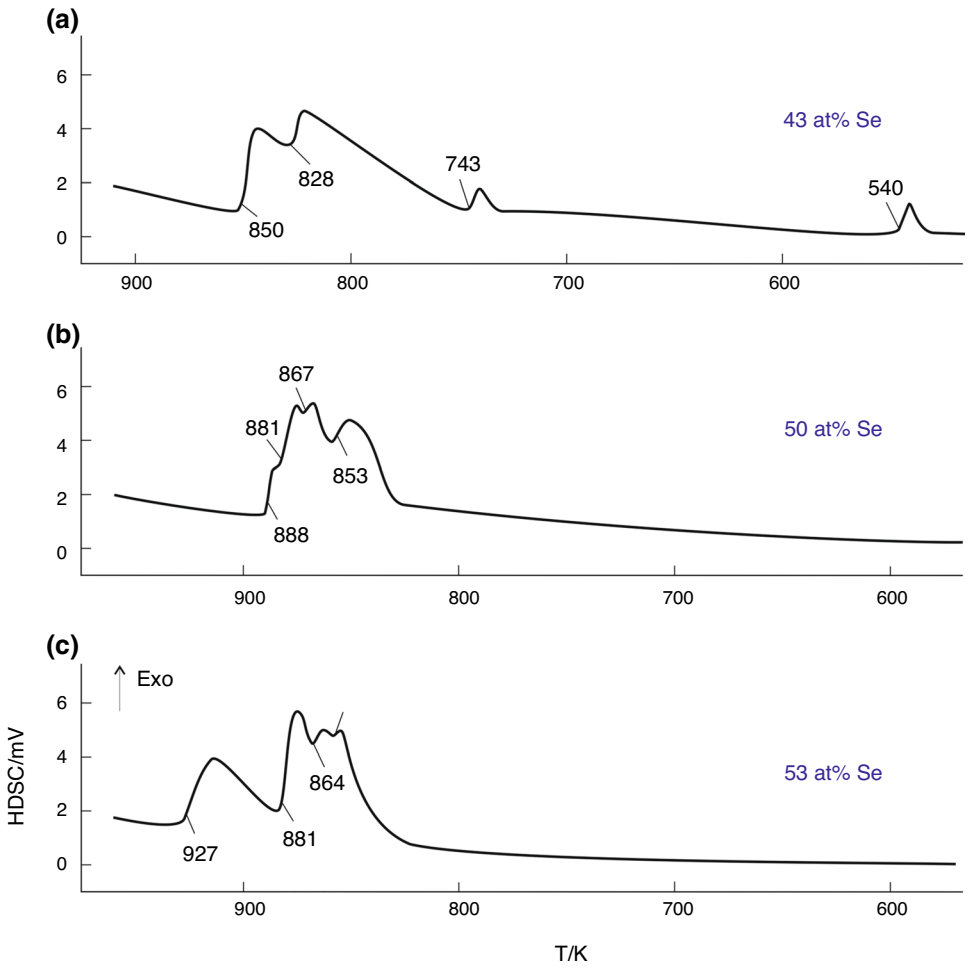

Fig. 7 DTA cooling curves of some samples

$$S^0\,(Bi_8Se_7) = \Delta\bar{S}_{\mathrm{Bi}} + S^0(Bi) + 7S^0(BiSe) \tag{12}$$

$$S^0\,(Bi_4Se_3) = \frac{4}{7}\Delta\bar{S}_{\mathrm{Bi}} + \frac{4}{7}S^0(Bi) + \frac{3}{7}S^0(Bi_8Se_7) \tag{13}$$

$$S^0\,(Bi_3Se_2) = \frac{1}{3}\Delta\bar{S}_{Bi} + \frac{1}{3}S^0(Bi) + \frac{2}{3}S^0(Bi_4Se_3) \tag{14}$$

the standard entropies of bismuth selenides were determined. The data obtained are shown in Table 5. In the calculations, we used the data of [40] on the standard entropy of bismuth (56.7 ± 0.5 J mol^{-1} K^{-1}) and selenium (42.1 ± 0.2 J mol^{-1} K^{-1}), as well as the standard integral thermodynamic functions of BiSe [49]. Errors were determined by the *error accumulation method.*

Table 5, in addition to the results of the present contribution, also shows the data obtained by us [49] for other bismuth selenides. It should be noted that a detailed comparative analysis of our and published data for the Bi_2Se_3 and BiSe compounds is given in [49].

Table 2 Primary data of EMF measurements for alloys from the $Bi_8Se_7 + BiSe$ $Bi_4Se_3 + Bi_8Se_7$ and $Bi_3Se_2 + Bi_4Se_3$ phase regions

T/K	E/mV		
	$Bi_8Se_7 + BiSe$	$Bi_4Se_3 + Bi_8Se_7$	$Bi_3Se_2 + Bi_4Se_3$
300.8	88.92	77.16	55.22
307.6	89.44	76.82	56.28
312.2	88.68	76.36	57.41
315.4	89.54	77.55	56.96
321.8	90.06	77.45	57.33
327.4	90.72	78.22	58.12
332.9	90.5	78.68	58.34
337.5	90.54	78.7	58.41
342.8	91.07	78.54	60.02
347.7	91.21	78.56	59.83
350.6	91.11	79.32	60.02
355.2	91.02	78.85	60.75
358.7	90.96	79.44	60.34
366.4	92.33	80.18	60.08
372.3	92.84	80.83	61.96
379.1	93.02	80.62	61.94
384.2	93.26	81.8	64.33
388.1	94.41	81.11	63.51
391.6	94.88	81.18	63.92
397.8	95.22	82.5	64.86
402.7	95.2	82.44	65.06
408.1	95.24	81.82	65.08
412.3	95.91	83.04	65.18
417.5	96.45	82.61	66.01
422.8	96.2	82.66	66.08
426.7	97.08	83.5	67.12
432.6	96.45	83.88	67.07
439.9	97.94	83.62	67.92
445.2	98.61	84.75	68.74
449.6	99.55	84.82	68.25

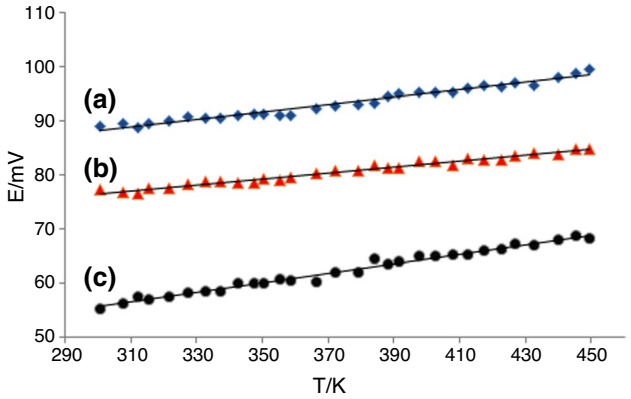

Fig. 8 Temperature dependences of the EMF of concentration cells (Eq. 1) for cathode phase assemblages **a** $Bi_8Se_7 + BiSe$, **b** $Bi_4Se_3 + Bi_8Se_7$, and **c** $Bi_3Se_2 + Bi_4Se_3$

Table 4 Relative partial functions of bismuth in the alloys of the Bi-Se system at 298 K

Phase area	$-\Delta\overline{G}_{Bi}$ kJ mol^{-1}	$-\Delta\overline{H}_{Bi}$	$\Delta\overline{S}_{Bi}$ J mol^{-1} K^{-1}
$Bi_8Se_7 + BiSe$	25.48 ± 0.08	19.57 ± 0.32	19.84 ± 0.85
$Bi_4Se_3 + Bi_8Se_7$	22.11 ± 0.06	17.38 ± 0.25	15.85 ± 0.65
$Bi_3Se_2 + Bi_4Se_3$	16.04 ± 0.07	8.42 ± 0.30	25.58 ± 0.78

Table 3 Temperature dependences of the EMF of chains type (1) for alloys of the Bi-Se system in the 300–450 K temperature range

Phase area	$E, mV = a + bT \pm 2[\delta_E^2/n + \delta_b^2(T - \overline{T})]^{1/2}$
$Bi_8Se_7 + BiSe$	$67.59 + 0.0685T \pm 2\left[\frac{0.28}{30} + 4.9 \times 10^{-6}(T - 374.92)\right]^{1/2}$
$Bi_4Se_3 + Bi_8Se_7$	$60.04 + 0.0548T \pm 2\left[\frac{0.16}{30} + 2.8 \times 10^{-6}(T - 374.92)\right]^{1/2}$
$Bi_3Se_2 + Bi_4Se_3$	$29.07 + 0.0884T \pm 2\left[\frac{0.24}{30} + 4.1 \times 10^{-6}(T - 374.92)\right]^{1/2}$

Table 5 Standard integral thermodynamic functions of bismuth selenides at 298 K

Compound	$-\Delta_f G^0(298K)$	$-\Delta_f H^0(298K)$	$\Delta_f S^0(298K)$	S°(298 K)
	kJ mol^{-1}		J mol^{-1} K^{-1}	
Bi_2Se_3 [49]	141.0 ± 0.2	139.6 ± 0.7	4.8 ± 1.8	245.1 ± 4.3
Bi_3Se_4 [49]	207.5 ± 0.3	204.5 ± 1.1	15.0 ± 2.7	349.5 ± 6.1
Bi_8Se_9 [49]	513.9 ± 0.8	500.3 ± 2.9	45.6 ± 4.4	880.2 ± 15.3
BiSe [49]	60.4 ± 0.1	58.5 ± 0.4	6.4 ± 0.6	105.6 ± 1.8
Bi_8Se_7	448.3 ± 0.8	429.1 ± 3.9	64.4 ± 5.1	815.0 ± 14.0
Bi_4Se_3	204.8. ± 0.4	193.8 ± 1.9	36.9 ± 5.0	391.0 ± 6.8
Bi_3Se_2	141.9 ± 0.3	132.0 ± 1.5	33.2 ± 3.6	288.1 ± 5.0

Conclusions

Using the DTA, XRD, and SEM methods, as well as measurements of the EMF of concentration chains relative to the bismuth electrode, we obtained a new set of mutually consistent data on the phase relationships and thermodynamic functions of the Bi-Se system. The constructed phase diagram represents the formation of the compounds Bi_2Se_3, Bi_3Se_4, Bi_8Se_9, BiSe, Bi_8Se_7, Bi_4Se_3, and Bi_3Se_2 with almost stoichiometric compositions. Except for Bi_2Se_3 with congruent melting at 978 K, the above-mentioned compounds melt with decomposition by peritectic reactions at 890, 881, 866, 853, 829, and 742 K, respectively. The partial Gibbs free energy, enthalpy, and entropy of bismuth in alloys, standard integral thermodynamic functions of formations, and standard entropies of bismuth selenides were calculated from the EMF measurements at equilibrium conditions.

Supplementary Information The online version contains supplementary material available at https://doi.org/10.1007/s10973-021-10975-0.

Acknowledgements The work has been carried out within the framework of the international joint research laboratory "Advanced Materials for Spintronics and Quantum Computing" (AMSQC) established between the Institute of Catalysis and Inorganic Chemistry of ANAS (Azerbaijan) and Donostia International Physics Center (Basque Country, Spain) and partially supported by the Science Development Foundation under the President of the Republic of Azerbaijan, a grant EİF/MQM/Elm-Tehsil-1-2016-1(26)-71/01/4-M-33.

References

1. Rowe DM. Thermoelectrics Handbook: Macro to Nano. Boca Raton, FL. CRC Press. Taylor & Francis Group; 2006
2. Shevelkov AV. Chemical aspects of the design of thermoelectric materials. Russ Chem Rev. 2008;77:1–19. https://doi.org/10.1070/RC2008v077n01ABEH003746.
3. Tumelero MA, Martins MB, Souza PB, Della Pace RD, Pasa AA. Effect of electrolyte on the growth of thermoelectric Bi_2Se_3 thin films. Electrochim Acta. 2019; 300: 357–62. https://doi.org/10.1016/j.electacta.2019.01.069
4. Adam AM, Elshafaie A, Mohamed AA, Petkov P, Ibrahim EMM. Thermoelectric properties of Te doped bulk Bi_2Se_3 system. Mater Res Express. 2018;5:035514–6. https://doi.org/10.1088/2053-1591/aab5e8.
5. Adam AM, Lilov E, Ibrahim EMM, Petkov P, Panina LV, Darwish MA. Correlation of structural and optical properties in as-prepared and annealed Bi_2Se_3 thin films. J Mater Process Tech. 2019;264:76–83. https://doi.org/10.1016/j.jmatprotec.2018.09.005.
6. Wang Q, Wu X, Wu L, Xiang Y. Broadband nonlinear optical response in Bi_2Se_3-Bi_2Te_3 heterostructure and its application in all-optical switching. AIP Adv. 2019;9:025022–7. https://doi.org/10.1063/1.5082725.
7. Lawal A, Shaari A, Ahmed R, Jarkoni N. First-principles many-body comparative study of Bi_2Se_3 crystal: a promising candidate for broadband photodetector. Phys Lett A. 2017;381:2993–9. https://doi.org/10.1016/j.physleta.2017.07.023.
8. Wang Y, Law S. Optical properties of $(Bi_{1-x}In_x)_2Se_3$ thin films. Opt Mater Express. 2018;8:2570–8. https://doi.org/10.1364/OME.8.002570.
9. Moore JE. The birth of topological insulators. Nature. 2010;464:194–8. https://doi.org/10.1038/nature08916.
10. Kane CL, Moore JE. Topological insulators. Phys World. 2011;24:32–6. https://doi.org/10.1088/2058-7058/24/02/36.
11. Politano A, Silkin VM, Nechaev IA, Vitello MS, Viti L, Aliev ZS, Babanly MB, Chiarello G, Echenique PM, Chulkov EV. Interplay of surface and Dirac plasmons in topological insulators: the case of Bi_2Se_3. Phys Rev Lett. 2015;115:216802–5. https://doi.org/10.1103/PhysRevLett.115.216802.
12. Flammini R, Colonna S, Hogan C, Mahatha S, Papagno M, Barla A, Sheverdyaeva PM, Moras P, Aliev ZS, Babanly MB, Chulkov EV, Carbone C, Ronci F. Evidence of β-antimonene at the Sb/Bi_2Se_3 interface. Nanotechnology. 2018;29:065704–7. https://doi.org/10.1088/1361-6528/aaa2c4.
13. Hogan C, Holtgrewe K, Ronci F, Colonna S, Sanna S, Moras P, Sheverdyaeva PM, Mahatha S, Papagno M, Aliev ZS, Babanly MB, Chulkov EV, Carbone C, Flammini R. Temperature driven phase transition at the antimonene/Bi_2Se_3 van der Waals heterostructure. ACS Nano. 2019;13:10481–9. https://doi.org/10.1021/acsnano.9b04377.
14. Mamedov NT, Alizade EH, Jahangirli ZA, Aliev ZS, Abdulayev NA, Mammadov SN, Amiraslanov IR, Shim Y, Wakita K, Ragimov SS, Bayramov AI, Babanly MB, Shikin AM, Chulkov EV. Infrared spectroscopic ellipsometry and optical spectroscopy of plasmons in classic 3D topological insulators. J Vac Sci Technol B. 2019;37:062602–6. https://doi.org/10.1116/1.5122776.
15. Politano A, Caputo M, Nappini S, Bondino F, Aliev ZS, Babanly MB, Chulkov EV. Exploring the surface chemical reactivity of single crystals of binary and ternary bismuth chalcogenides. J Phys Chem C. 2014;118:21517–22. https://doi.org/10.1021/jp506444f.
16. Wang Z, Gao XPA, Zhang Z. Transport properties of doped Bi_2Se_3 and Bi_2Te_3 topological insulators and heterostructures. Chin Phys B. 2018;27:107901–9. https://doi.org/10.1088/1674-1056/27/10/107901.
17. Yonezawa S. Nematic superconductivity in doped Bi_2Se_3 topological superconductors. Condens Matter. 2019;4:2–20. https://doi.org/10.3390/condmat4010002.
18. Walsh LA, Smyth CM, Barton AT, Wang Q, Che Z, Yue R, Kim J, Kim MJ, Wallace RM, Hinkle CL. Interface chemistry of contact metals and ferromagnets on the topological insulator Bi_2Se_3. J Phys Chem C. 2017;121:23551–63. https://doi.org/10.1021/acs.jpcc.7b08480.
19. Viti L, Coquillat D, Politano A, Kokh KA, Aliev ZS, Babanly MB, Tereshchenko OE, Knap W, Chulkov EV, Vitiello MS. Plasma-Wave terahertz detection mediated by topological insulators surface states. Nano Lett. 2016;16:80–7. https://doi.org/10.1021/acs.nanolett.5b02901.

20. Babanly MB, Chulkov EV, Aliev ZS, Shevelkov AV, Amiraslanov IR. Phase diagrams in materials science of topological insulators based on metal chalcogenides. Russ J Inorg Chem. 2017;62:1703–29. https://doi.org/10.1134/S0036023617130034.
21. Imamaliyeva SZ, Babanly DM, Tagiev DB, Babanly MB. Physicochemical aspects of development of multicomponent chalcogenide phases having the Tl_5Te_3 structure: a review. Russ J Inorg Chem. 2018;63:1703–30. https://doi.org/10.1134/S0036023618130041.
22. Babanly MB, Mashadiyeva LF, Babanly DM, Imamaliyeva SZ, Taghiyev DB, Yusibov YA. Some issues of complex investigation of the phase equilibria and thermodynamic properties of the ternary chalcogenide systems by the EMF method. Russ J Inorg Chem. 2019;13:1649–71. https://doi.org/10.1134/S0036023619130035.
23. Matsushita T, Mukai K. Chemical thermodynamics in materials science: From Basics to Practical Applications. Springer; 2018.
24. Hansen M, Anderko K. Constitution of binary alloys. 2nd ed. New York: McGraw-Hill; 1958.
25. Parravano N. The system: bismuth-selenium. Gazz Chim Ital. 1913;43:201–9.
26. Tomoshige N. Metallographic investigation of the system Bismuth-selenium. Mem Coll Sci Kyoto Imp Univ. 1919;4:55–60.
27. Abrikosov NKh, Bankina VF, Kharitonovich KF. Phase diagram of the Bi-Se system. Russ J Inorg Chem. 1960;5:978–82.
28. Gather B, Blachnik R. Ternary systems containing chalcogenides. II The Gold-Bismuth-Selenium System Z Metallkd. 1975;66:356–9.
29. Godovikov AA. X-ray diffraction investigation of individual representatives of the Bi−Se system. J Struct Chem. 1962;3:38–43. https://doi.org/10.1007/BF00745376.
30. Langston SA, Lewis B. Compounds with the C33 tetradymite-type structure. J Phys Chem Solids. 1963;24:1387–9. https://doi.org/10.1016/0022-3697(63)90190-2.
31. Sher AA, Odin IE, Novoselova AV. Investigation of the phases in the Bi-Se system. Russ J Inorg Chem. 1986;31:435–7.
32. Semiletov SA, Pinsker ZG. Electronographic investigation of the bismuth–selenium system. Dokl Akad Nauk SSSR. 1955;100:1079–81.
33. Nakajima S. The crystal structure of $Bi_2Te_{3-x}Se_x$. J Phys Chem. 1963;24:479–85.
34. Stasova MM. Crystal structure of bismuth selenides and bismuth and antimony tellurides. Zh Strukt Khim. 1967;8:584–9.
35. Stasova MM. Crystal structure of the bismuth selenide Bi_4Se_3. J Inorg Mater. 1968;4:21–3.
36. Imamov EM, Semiletov SA. The crystal structure of the phases in the systems Bi-Se, Bi-Te, and Sb-Te. Sov Phys Crystallogr. 1971;15:845–50.
37. Gardes B, Brun G, Tedenac J-C. Contribution to the study of the bismuth-selenium system. Eur J SolidState Inorg Chem. 1989;26:221.
38. Okamoto H. The Bi-Se (Bismuth-Selenium) system. J Phase Equil. 1994;15:195–201. https://doi.org/10.1007/BF02646366.
39. Barin I. Thermochemical Data of Pure Substances. 3rd Ed. Wiley-VCH Verlag GmbH & Co.; 2008.
40. Database of thermal constants of substances. Digital version. Eds.: V.S. Iorish and V.S. Yungman. 2006. http://www.chem.msu.ru/cgi-bin/tkv.pl
41. Kubaschewski O, Alcock CB, Spenser PJ. Materials thermochemistry. Oxford: Pergamon Press; 1993.
42. Mills KC. Thermodynamic data for inorganic sulphides, selenides, and tellurides. London: Butterworth; 1974.
43. Melekh BT, Semenkovich SA. Thermodynamic properties of bi (iii) telluride and selenide. Inorg Mater. 1968;4:1180–2.
44. Vasil'ev VP, Somov AP, Nikol'skaya AV, and Gerasimov YaI. Thermodynamic Properties of Bismuth Selenide from EMF Measurements. Zh. Fiz. Khim., 1968; 42: 675–7.
45. Sidorko VR, Goncharuk LV, Antonenko RV. Thermodynamic properties of bismuth sesquiselenide and sesquitelluride and their solid solutions. Powder Metall Met C. 2008; 47: 234–41. https://doi.org/10.1007/s11106-008-9009-3.
46. Glazov VM, Pavlova LM, Gaev DS. Thermal stability of the selenides of the elements of groups iv and v of the periodic system, from the data on the curvature of the liquidus at the melting point. Russ J Inorg Chem. 1984;29:620–4.
47. Antipov AV, Rudnyi EB, Dobrokhotova ZhV. Thermodynamic Evaluation of the Bi–Se System. Inorg Mater. 2001;37:126–32. https://doi.org/10.1023/A:1004145224273.
48. Chen Y, Liu Y, Chu M, Wang L. Phase diagrams and thermodynamic descriptions for the Bi–Se and Zn–Se binary systems. J Alloy Compd. 2014;617:423–8. https://doi.org/10.1016/j.jallcom.2014.08.001.
49. Hasanova GS, Aghazade AI, Babanly DM, Tagiev DB, Yusibov YuA, Babanly MB. Thermodynamic properties of bismuth selenides. Russ. J. Phys. Chem. 2021; 95: 920–5. https://doi.org/10.1134/S0036024421050137.
50. Abrikosov NK, Bankina VF, Poretskaya LV, Shelimova LE, Skudnova EV. Semiconducting II–VI, IV–VI, and V-VI Compounds. US: Springer; 1969.
51. Brebrick RF. Characterization of phases in the 50–60 at. % Te region of the Bi–Te system by X-ray powder diffraction patterns. J. Appl. Cryst. 1968; 1: 241–6. https://doi.org/10.1107/S0021889868005406.
52. Wagner C. Thermodynamics of alloys. 1st ed. Boston: Addison-Wesley Press; 1952.
53. Morachevsky AG, Voronin GF, Geyderich VA, Kutsenok IB. Electrochemical research methods in the thermodynamics of metallic systems. Moscow: Akademkniga Publ; 2003. **(in Russian)**.
54. Babanly MB, Yusibov YA, Babanly NB. In: S.Kara (ed.). Electromotive force and measurement in several systems. IntechOpen. 2011. DOI: 10.5772/28934
55. Vassiliev VP, Lysenko VA. New approach for the study of thermodynamic properties of lanthanide compounds. Electrochim Acta. 2016;222:1770–5. https://doi.org/10.1016/j.electacta.2016.11.075.
56. Vassiliev V, Gong W. Electrochemical Cells with the liquid electrolyte in the study of semiconductor, metallic and oxide systems. In electrochemical cells – new advances in fundamental researches and applications. Ed.Yan Shao. IntechOpen; 2012; 71–102. https://doi.org/10.5772/39007.
57. Babanly NB, Orujlu EN, Imamaliyeva SZ, Yusibov YA., Babanly MB. Thermodynamic investigation of silver-thallium tellurides by EMF method with solid electrolyte Ag_4RbI_5. J Chem Thermodyn. 2019; 128: 78–86. https://doi.org/10.1016/j.jct.2018.08.012.
58. Alverdiev IDzh, Imamalieva SZ, Babanly DM, Yusibov YuA, Tagiev DB, Babanly MB. Thermodynamic study of siver–tin selenides by the EMF method with Ag_4RbI_5 solid electrolyte. Russ J Electrochem. 2019; 55: 467–74. https://doi.org/10.1134/S1023193519050021.
59. Moroz MV, Prokhorenko MV, Prokhorenko SV, Yatskov MV. Thermodynamic properties of $AgIn_2Te_3I$ and $AgIn_2Te_3Br$ determined by EMF method. Russ J Phys Chem. 2018;92:19–23. https://doi.org/10.1134/S0036024418010168.
60. Moroz M, Tesfaye F, Demchenko P, Prokhorenko M, Lindberg D. Phase equilibria and thermodynamics of selected compounds in the Ag–Fe–Sn–S system. J Electron Mater. 2018;47:5433–42. https://doi.org/10.1016/j.solidstatesciences.2020.106344.

61. Jain A, Kandan R. Determination of the thermodynamic stability of europium boride (EuB6). J Therm Anal Calorim. 2018;132:275–83. https://doi.org/10.1007/s10973-017-6876-1.
62. Mukherjee S, Dawar R, Phapale S, Dash E, Mishra R. Thermodynamic stability of CaThF6(cr) by transpiration and e.m.f. techniques. J Therm Anal Calorim. 2019;137:667–77. https://doi.org/10.1007/s10973-018-7950-z.
63. Imamaliyeva SZ, Mekhdiyeva IF, Babanly DM, Zlomanov VP, Tagiyev DB, Babanly MB. Solid-phase equilibria in the system Tl_2Te–Tl_2Te_3–$TlErTe_2$ and thermodynamic properties of the compounds Tl_9ErTe_6 and $TlErTe_2$. Russ J Inorg Chem. 2020;65:1762–9. https://doi.org/10.1134/S0036023620110066.
64. Osadchii EG, Korepanov YI, Zhdanov NN. A multichannel electrochemical cell with glycerin-based liquid electrolyte. Instrum Exp Tech. 2016;59:302–4. https://doi.org/10.1134/S0020441216010255.
65. Imamaliyeva SZ, Babanly DM, Gasanly TM, Tagiev DB. Thermodynamic properties of Tl_9GdTe_6 and $TlGdTe_2$. Russ J Phys Chem A. 2018;92:2111–6. https://doi.org/10.1134/S0036024418110158.
66. Babanly DM, Aliev ZS, Majidzade VA, Tagiyev DB, Babanly MB. Experimental study of phase equilibria and thermodynamic properties of the Tl–Se–I system. J Therm Anal Calorim. 2018;134: 1765–73 https://doi.org/10.1007/s10973-018-7677-x
67. Aliev ZS, Musayeva SS, Imamaliyeva SZ, Babanlı MB. Thermodynamic study of antimony chalcoiodides by EMF method with an ionic liquid. J Therm Anal Calorim. 2018;133:1115–20. https://doi.org/10.1007/s10973-017-6812-4.
68. Imamaliyeva SZ, Musayeva SS, Babanly DM, Jafarov YI, Tagiyev DB, Babanly MB. Determination of the thermodynamic functions of bismuth chalcoiodides by EMF method with morpholinium formate as electrolyte. Thermochim Acta. 2019;679:178319–27. https://doi.org/10.1016/j.tca.2019.178319.
69. Brigouleix C, Anouti M, Jacquemin J, Caillon-Caravanier M, Galiano H, Lemordant D. Physicochemical characterization of morpholinium cation based protic ionic liquids used as electrolytes. J Phys Chem B. 2010;114:1757–66. https://doi.org/10.1021/jp906917v.